Progress In Electromagnetics Research C, Vol. 105, 117–128, 2020

A Grating-Coupled Plasmon Index Sensor Observing the 0th Reflection Carefully and Sensibly for Recognizing the Resonance Curve with the Absorption Center: The Existing State of Affairs Aiming for Seven-Digit Resolution

Xun Xu[1, 2, *], Miaoning Zheng[3], and Yoichi Okuno[3]

Abstract—First of all we inform the audiences that this article is a Review Paper (RP) for the PIERS17 Proceedings Paper (Zheng et al. [17]). The reason why we publish this RP is that: although the paper [17] reported important ideas and simulation facts, details of the contents were insufficient, and the audiences of the report were not satisfied. This was because the page number was limited, and we saved the number of pages. However, because the contents of [17] are important, we decided to publish an RP, which would provide additional explanations or give considerations supporting main issues. Now, we start the abstract from Section 1. Here, we mention historical topics and RP-related things. In Section 2, we explain the problem of diffraction by a conically-mounted metal grating. To save the page number, we skip the method of solution. In Section 3, we explain our method in noise free case. We show the high precision of the quadratic (or parabola) approximation. We define the workspace (WS: relation between index range of a sample and a proper azimuth angle) and one-to-one correspondence between sample index and resonance angle. In Section 4, we try our method in a noisy environments. A curve-fitting procedure and three types of noise filters work to find satisfactory solutions. That is, in both 3. and 4., the resolution of the index is 7-digit usually, which is our target from the beginning. We think that the introduction of AI or statistical processing would increase the stability of the result. In Section 5, we mention some of future works. In APPENDIX A, we explain the method: How to find the azimuth angle, which we need in solving the diffraction problems by conically-mounted grating.

1. INTRODUCTION

When a metal grating is illuminated by a TM(p)-polarized light, absorption of the incident light occurs at a specific angle of incidence θ_r, which is called resonance angle. This phenomenon is referred to as plasmon resonance absorption (PRA), which is caused by the excitation of plasmon surface waves and is accompanied by an abrupt change (usually a dip) of the reflection efficiency [1–5]. It is known that the resonance angle is a sensitive function of the refractive index of the liquid material that occupies V_1, the half space whose lower surface borders are on the grating surface.

By the way, it is also widely known that metal gratings have the problem of Wood's anomaly, and again, in the TM incidence, the anomaly spoils the performance of the gratings. It was discovered by Wood in 1902 [6] and the discussions on the character of anomaly and countermeasures by Rayleigh [7] and Fano [8], and others continued until recently. The recent discussions included the similarity between the plasmon and the anomaly [2, 9]. In this connection, we remember that the last 20 or 30 years of the

Received 21 April 2020, Accepted 3 September 2020, Scheduled 13 September 2020
* Corresponding author: Xun Xu (xunamane@gmail.com).
[1] Centre for Optical and Electromagnetic Research, Zhejiang University (COER-ZJU), Hangzhou 310058, China. [2] Kurume Institute of Technology, Kurume 830-0052, Japan. [3] Centre for Optical and Electromagnetic Research, South China Normal University (COER-SCNU), Guangzhou 510006, China.

20th Century were the beginning of the Nano-Technology (Nanotech, Nanotechnologies). The following is a famous story: Prof. Taniguchi (Science Univ. Tokyo) used the word "Nano-Technology" for the first time [10], and he said "the processing accuracy in the 21st Century must be 1 nm". We should say: a quick temper might be the only defect in his character. Anyway, we should utilize one edge or a single part of the Nanotech in designing a prototype. Because the present article is something like a draft of the prototype of our sensor kept in a computer, we can try our ideas. If we get good results, we will equip that function in an actual prototype.

Now, we go back to the original way, and let us confirm our target. We already mentioned it in the title, and here we would like to provide additional explanations. We are a small group participating in the issue of grating-coupled refractive index sensors from the viewpoint of Computational Electromagnetics (CEM). We guess that a huge number of researchers and students are working in Nanotechnologies. A considerable number of them are developing index sensors [11, 12] as an application of the PRA event. Although the application seems easy, actual development of an index sensor requires much time and effort. The source of this issue might be the high specification in resolution.† We hope to achieve 7-digit resolution in the refractive index. This requires no less than 6 or 7 significant figures of the resonance angle θ_r in degrees. Thus, we face many problems in finding the precise location of θ_r. Some of the representative causes are: lack of instrumental resolution (IR), the efficiency curves beyond our control, inconvenient reflected beams (in strength, half-width, etc.), etc. Therefore, it is not an easy work to develop a required index sensor. Although we basically follow the above phenomenon, we should find and use some innovative idea to attain our goal. In the last few years (from 2017 through 19), we have found a couple of important points from the results of computer simulations, the points which help us to achieve our target (7-digit resolution). We think publication of the points together with related knowledge may help the people working in sensor application of Plasmonics. We do not know how helpful we could be, but we would like to do our best.

We may have to explain our computational method for solving the diffraction problems. This is called Yasuura's method of modal expansion (YM). Basically, this is a simple and fast method, but the present problem is formulated in pseudo 3D, and the computer program must be complicated. Fortunately, one of the authors (Y.O.) published a joint-authorship chapter recently on introduction to the YM with applications to grating problems [13]. In addition, a couple of former colleagues published a paper on their status in sensor development [14]. These two articles must be good for interested readers. In particular, the latter is convenient for newcomers to the CEM because: (a) Their problem is common to ours in the present article; (b) Most of the variables and symbols are also common. Hence, we decided that: after formulating the EM problem in Section 2, we move to Section 3 without explaining our method of solution. Although the method is rather complicated, it is not difficult at all. In addition to the two references above, some of our recent publications in PIERS [15–18] may serve well. As for our rating of the YM, please consult the footnote.‡

Before closing this section, we would like to provide some additional explanation and our opinion. As we pointed out, the proceedings paper [17] is too short and vague sometimes. We think that it is for a short range. Instead, we hope that this article has an opposite nature: enough space and free from confusion or doubt. We hope this and endeavor to attain.

2. FORMULATION OF THE DIFFRACTION PROBLEM

Figure 1(a) shows the geometry of conical diffraction by a metal grating. We employ a grating with sinusoidal surfaces S_1 and S_2 given by

$$z_1 = h \sin 2\pi x/d; \quad z_2 = z_1(x) - e, \tag{1}$$

where $(x,\ z_1)$ and $(x,\ z_2)$ are points (or straight lines in Y-direction) on the surfaces S_1 and S_2. The grating shape is assumed sinusoidal and can be replaced by a Fourier grating in a completed version.

† We have heard 7- or 8-digit resolution [minimum indicate value 1E(−6) or 1E(−7)] was required by Clinical Medicine, Physiology, and others. Comparison with the light speed, we supposed that 8-digit would be a very high target. Thus we took a refractometer type 7-digit sensor, which might be a little more realistic and could be our goal.

‡ The power of the YM is average so long as usual modal functions (MF) (e.g., Floquet) are used as MF. But, if one uses MF whose combinations can represent the boundary condition easier, the person gets good solution with a small number of MF. The reason why we choose the YM is that we have used it for more than 40 years.

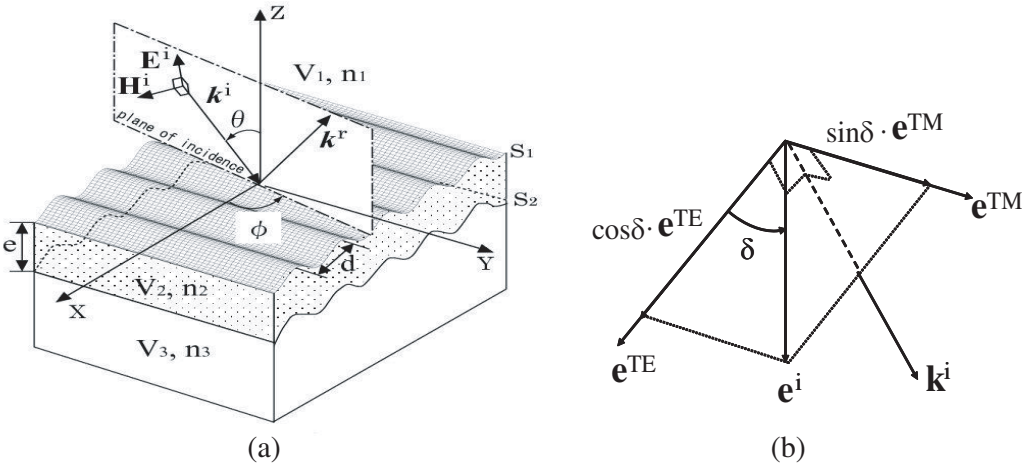

Figure 1. (a) Conical diffraction of a TM (p) polarized incident light by a metal grating. V_1 is a semi-infinite region over the grating surface and is occupied by a sample material whose relative index is n_1. V_2 is a gold over-coating (thickness e) and V_3 is a holographic grating made of aluminum. The surfaces S_1 and S_2 are corrugated sinusoidally in X with a period d and a depth $2h$. The plane of incidence makes an azimuth angle ϕ with the direction of periodicity X. θ is an incident zenith angle and the electric field of the incident light is parallel to the plane. If e is sufficiently thick (a few hundred nm), we can neglect the aluminum layer together with the boundary S_2 (b) Definition of a polarization angle δ.

We assume that the incident wavelength λ is a little greater than the grating period d, so that there is only one propagating order ($m = 0$) in the majority of the zenith angle range.[§] The incident light is given by

$$\begin{bmatrix} \mathbf{E}^i \\ \mathbf{H}^i \end{bmatrix}(\mathbf{r}) = \begin{bmatrix} \mathbf{e}^i \\ \mathbf{h}^i \end{bmatrix} \exp(i\mathbf{k}^i \cdot \mathbf{r} - i\omega t). \tag{2}$$

Here, $\mathbf{e}^i$ and $\mathbf{h}^i$ are electric- and magnetic-field amplitudes of the incident light [See Figure 1(b)]. They satisfy

$$\mathbf{h}^i = (\omega\,\mu_0)^{-1}\mathbf{k}^i \times \mathbf{e}^i, \tag{3}$$

and $\mathbf{k}^i$ is the incident wavevector given by

$$\mathbf{k}^i = n_1 k(\sin\theta\cos\phi, \sin\theta\sin\phi, -\cos\theta) = (\alpha_0, \beta, -\gamma_0) \tag{4}$$

with θ being the zenith angle between k^i and the grating normal $\mathbf{u}_Z$. The $\mathbf{e}^i$ and $\mathbf{h}^i$ carry the information of polarizations: TM(p) and TE(s). To show this clearly, we define two unit vectors that span a plane orthogonal to the incident wavevector $\mathbf{k}^i$:

$$\mathbf{e}^{\mathrm{TE}} = (\sin\phi, -\cos\phi, 0), \quad \mathbf{e}^{\mathrm{TM}} = (\cos\theta\cos\phi, \cos\theta\sin\phi, \sin\theta). \tag{5}$$

Combining the two vectors in Eq. (5), we represent the electric-field amplitude as

$$\mathbf{e}^i = \mathbf{e}^{\mathrm{TE}}\cos\delta + \mathbf{e}^{\mathrm{TM}}\sin\delta, \tag{6}$$

where δ is a polarization angle (see Fig. 1(b)). We set $\delta = \pi/2$ in the following because we use a TM polarized incident wave. The time factor $\exp(-i\omega\,t)$ will be suppressed throughout.

Now we can state the problem to seek the diffracted electric- and magnetic-fields in the three regions:

Problem 1. Find the diffracted waves ($\mathbf{E}_R$, $\mathbf{H}_R$) in V_R ($R = 1$, 2, and 3) that satisfy the following conditions (In conical mounting, the EM fields in each region have both TM- and TE-components, e.g., $\mathbf{E}_1 = \mathbf{E}_1^{\mathrm{TM}} + \mathbf{E}_1^{\mathrm{TE}}$):

[§] Only the 0th-order TM- and TE-modes are always propagating. This choice is for simplicity: the optimization of grating profile (including the period d) would be the next issue in our mid-term plan.

(a) The homogeneous Helmholtz equation in each region;
(b) The 1D radiation condition in V_1 and in V_3;
(c) Periodicity conditions that: any component $f(X, Y, Z)$ of the diffracted waves satisfies the relation $f(X + d, Y, Z) = \exp(i\alpha_0 d) f(X, Y, Z)$, and the phase constant in Y is β constantly;
(d) The boundary conditions on S_1 and S_2 that the total tangential components of electric- and magnetic-fields are continuous across the two boundaries.

We mentioned in Section 1 that we employ the YM in solving **Prob. 1** and that we do not go deeper into the method in this article. We hope that interested readers get necessary information from the references cited at the end of Section 1.

3. NUMERICAL EXAMPLES AND DISCUSSION (I): WITHOUT NOISE

3.1. Physical Parameters in Numerical Analysis and Examples of Typical Plasmon Excitation

Here we list the physical parameters employed in our numerical analysis. The majority of the parameters are taken from catalogues of optical devices and systems published by Nanotech Companies. The others are similar to catalogue data, but slightly modified sometimes to satisfy our convenience. The grating parameters[‖] are $2h = 61\,\text{nm}$ (depth), $d = 556\,\text{nm}$ (period), and $e = 44\,\text{nm}$ (gold layer thickness). The incident light is a monochromatic TM plane wave with $\lambda = 660\,\text{nm}$. Refractive indices of gold and aluminum at this wavelength are $n_2 = 0.1355 + i3.4679$ and $n_3 = 1.3517 + i7.1150$. We postulate that these values are correct throughout the whole effective digits: That is, if we use a 7 significant digits system, we put $n_2 = 0.135500 + i3.467900$, and so on. In this connection, let us define a parameter (a rough approximation of the sample index n_1), which will play an important role in our method. Here, rough means 4- or 5-digit, and we take 4 in this paper: if $n_1 = 1.234567$, then $n_{1,rough} = 1.235$.

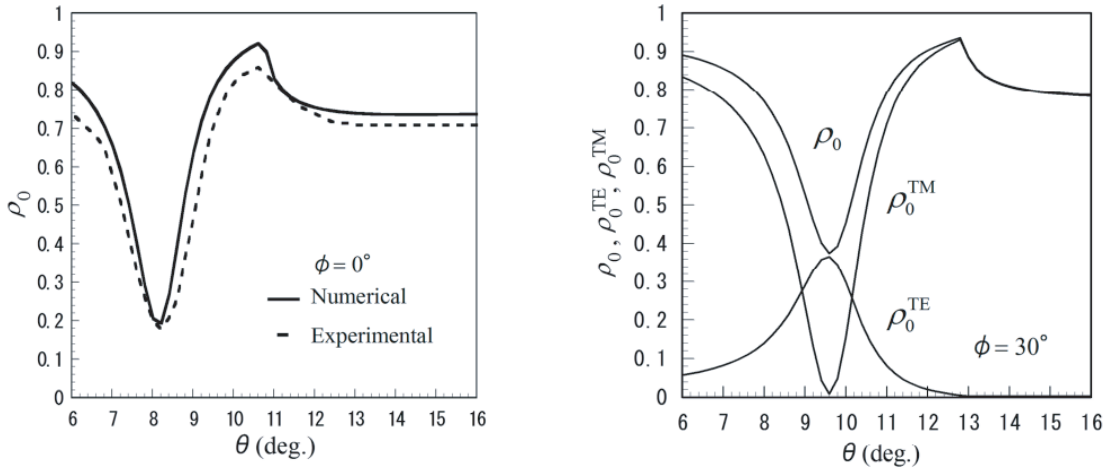

Figure 2. Typical resonance absorption in planer and conical mounting: (a) Planer mounting (TM incidence, $n_1 = 1.0$, and $\phi = 0$; (b) Conical mounting (TM incidence, $n_1 = 1.0$, and $\phi = 30°$).

Figures 2(a) and 2(b) show typical PRA's: 2(a) planer mounting; and 2(b) conical mounting. In Fig. 2(a), we observe the 0th reflection efficiency $\rho_0(\theta) = \rho_0^{\text{TM}}(\theta) = |A_{1,0}^{\text{TM}}(\theta)|^2$, where $\theta = \theta^i$ and $A_{1,0}^{\text{TM}}$ is one of the modal coefficients.[¶] Because this is a scalar 2D problem, we have no mode conversion here.

[‖] This original was a UV grating made of Al with an Au over-coating. The original grooving was 1,800 g/mm. We have neglected the harmonics from the original profile because the optimization of parameters belongs to our future issues. By the way, we should check the postulates or assumptions relating to the metal index value and, if necessary, cope with a problem caused by the assumptions [18]. This report mentioned four sources [19–22] of Au indices.

[¶] Let the solution in V_1 be $\mathbf{E}_1 = \mathbf{E}_1^{\text{TM}} + \mathbf{E}_1^{\text{TE}}$. Then, this is the coefficient of the 0th modal function of $\mathbf{E}_1^{\text{TM}}$.

The dip at $\theta = 8.2°$ shows the PRA, and the peak at 10.6° is caused by the -1 order cutoff. Fig. 2(b) shows what happens when the resonance absorption occurs in conical mounting. The resonance angle is $\theta_r = 9.6°$, and the cutoff is 12.8°. The biggest difference from Fig. 2(a) is the appearance of the TE_0-mode near the resonance angle. Because the incident light is polarized in TM, this means occurrence of the TM-TE mode conversion [23, 24]. Hence, this is a quasi 3D vector problem. Probably, the mode conversion occurs for satisfaction of the boundary conditions: because a greater part of the TM component is lost by the resonance absorption, the TE component appears to supply the deficiency. Note that the zenith angles corresponding to the extremes $\{\min(\rho_0^{\mathrm{TM}})\min(\rho_0)$, and $\max(\rho_0^{\mathrm{TE}})\}$ are slightly different from each other. The degree of difference depends on a variety of conditions.

3.2. Computation Results of a Resonance Curve near θ_r and a Quadratic Approximation

We have found through a systematic numerical survey that the curve of 0th-order TM reflection efficiency ρ_0^{TM} carries most of the information about the location of θ_r, the location closely related to n_1. On the contrary, we found almost no interesting result from the reflected TE_0 mode in the present setting. Because we often mention a distinctive part of the efficiency curve including $\theta = \theta_r$, we designate that part as a resonance curve $(\mathrm{RC})^+$ in the following discussions. Now, we show an example of the RC and an approximation by a quadratic (or parabola, second-order polynomial) curve, which also plays an important role in our method.

Both Figs. 3(a) and 3(b) illustrate two curves: the RC near the θ_r (blue solid curve) and its approximation by a quadratic function (red broken curve). Note that the former is a numerical solution of **Prob 1** obtained by the YM, while the latter is generated from the former by using the following conjecture (**C**) and procedures (**P**).

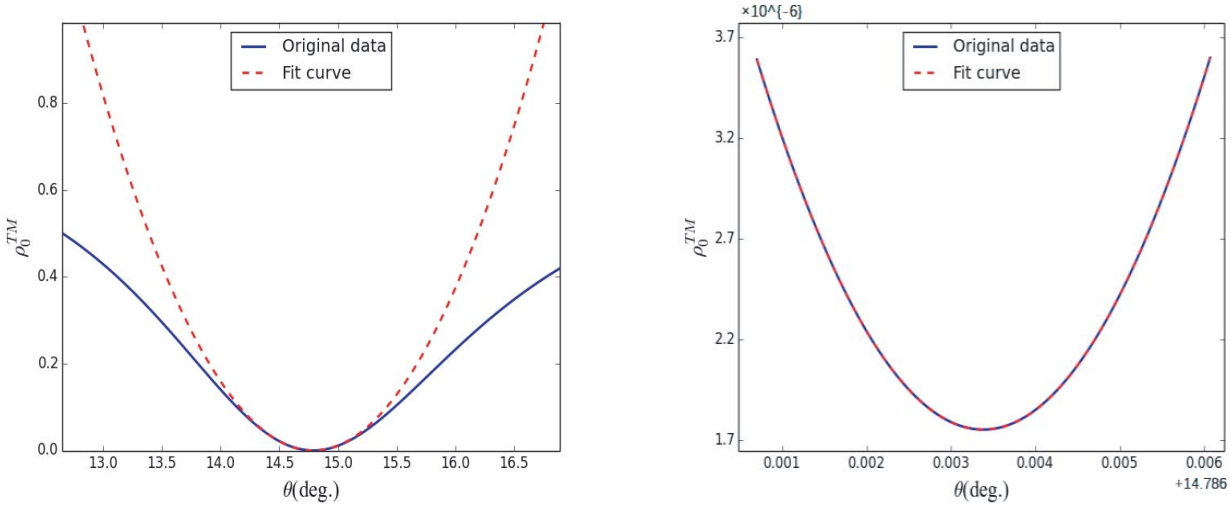

Figure 3. A resonance curve (RC) and its approximation ($n_{1,rough} = 1.306$, $\phi = 29.73°$, $n_1 = 1.306000$): (a) shows the RC obtained by the YM (blue, solid curve) and an approximation by a quadratic function (red, broken line); (b) illustrates an enlarged bottom part of (a). Enlargement ratios on the abscissa and ordinate are 7E2 ($\simeq 700$) and 5E5 ($= 500,000$), respectively. Hence, the area of (b) is an extremely small area of (a). In getting the approximation, we employed the least-squares method (LSM): additional explanations can be found in Section 4.

(**C**) In the close vicinity of θ_r [like the area in Fig. 3(b)], the quadratic approximation is quite effective to represent the RC precisely (as if the principal term of the RC near θ_r is a quadratic function of θ or its equivalence).

$^+$ There are many objects called RC. In this article, we mean: (i) a part of 0th-order TM reflection efficiency as a function of θ; (ii) including θ_r; and (iii) representing the features of the efficiency curve near θ_r.

(**P1**) How to get the blue RC in Fig. 3(a): (i) Get the rough index $n_{1,rough}$; (ii) Prepare the minimal efficiency value $\min[\rho_0^{\mathrm{TM}}(\theta_r)]$ of one's desire; (iii) Follow the procedure in APPENDIX A, and get the azimuth ϕ; (iv) Solve **Prob. 1** with ϕ by the YM, and draw the blue RC in Fig. 3(a).

(**P2**) How to find the red approximations in Fig. 3(a): Find the parabola part of the blue RC in Fig. 3(a); represent this result in a closed form. How to do in Fig. 3(b): Draw the red curve in Fig. 3(a); set the scales for Fig. 3(b); put the blue and red curves in Fig. 3(b).

Now, we observe Fig. 3 again. We notice in Fig. 3(a) that the two curves are close to each other in the bottom area, i.e., near the resonance angle θ_r. Fig. 3(b) is an expanded version of the bottom area and illustrates the area in detail. Although there are two curves (blue and red) also in Fig. 3(b), we observe only one purple curve there. This is because the two curves overlap each other, and we find almost perfect agreement near the bottom (i.e., θ_r) of the RC. Please confirm that blue curve is obtained by the YM, and the red curve is a parabola approximation. According to our trial computations, the approximation power of quadratic functions seems valid in every conceivable case. Of course, the range of validity or the strength of this phenomenon depends on the existing conditions. However, if we are looking for the resonance angle θ_r and if the quadratic approximation works well, let us employ the method with the conjectured approximation because it is an easy way to determine the location of θ_r with high accuracy.

3.3. Workspace and Estimation of Resolution

When measuring the index n_1 of a sample by our method, we first need to find the rough index value $n_{1,rough}$ (a four-digit approximation). It is easy by using a refractometer. Then, we make some computation to find a recommended azimuth angle ϕ. Before making this, we should have a candidate of $\min = \min[\rho_0^{\mathrm{TM}}(\theta_r)]$, which we should choose when getting the angle ϕ. Having made these preparations we can visit APPENDIX A to learn how to obtain the azimuth angle.

Getting the recommended angle, we can start the main part of computation (solving **Prob. 1**) under the constraint in the azimuth. However, we usually record the azimuth and a range of the rough n_1 for which the newly obtained azimuth is available. The Workspace (WS) is made in that way, which extends the area coverage of our sensor. The structure of each WS is a combination of [an index range] and [a recommended azimuth], which takes a form like $[1.320, 1.322)|29.53^\circ = (1.320 \leq n_{1,rough} < 1.322)|\phi = 29.53^\circ)$. If we make an accumulation of WS, we have something like Table 1. In addition, there is Table 2 below Table 1, which shows one-to-one correspondence between the resonance angle θ_r and the sample index n_1.

Table 1. An example of a table of WS's. Each WS is a combination of index range ($1.320 \leq n_{1,rough} < 1.322$) and recommended azimuth ($\phi = 29.53^\circ$). The width of a WS range is between 2E(−3) and 3E(−3).

Index range	Azimuth ϕ (deg.)	Index range	Azimuth ϕ (deg.)
[1.320, 1.322)	29.53	[1.310, 1.313)	29.63
[1.318, 1.320)	29.55	[1.308, 1.310)	29.65
[1.315, 1.318)	29.57	[1.305, 1.308)	29.70
[1.313, 1.315)	29.60		

Table 2. One-to-one correspondence of θ_r and $n_{1(}n_{1,rough} = 1.306$, $\phi = 29.73^\circ$).

n_1	θ_r (deg.)	n_1	θ_r (deg.)	n_1	θ_r (deg.)
1.306000	14.7893818	1.306003	14.7896304	1.306006	14.7898790
1.306001	14.7894647	1.306004	14.7897133	1.306007	14.7899620
1.306002	14.7895475	1.306005	14.7897962	1.306008	14.7900448

Using the information to draw a figure, we have Fig. 4, which shows the one-to-one relationship, again. This is an extremely enlarged picture, and we see the linear relation between θ_r and n_1 clearly, the relation which contributes the high resolution. The proportional constant plays an important role in examining the resolution. Because that is the most important target, we would like to discuss this subject again in the next occasion. Here, we briefly guess the resolution of our system. We employ two methods of estimation (**EM**) and explain both of them briefly.

(**EM1**) **Method using the relation between $\Delta\theta_r$ and Δn_1.** In this method form is important. From the proportional connection in the caption of Fig. 4, we have $\Delta n_1 = \Delta\theta_r/82.9$. If we employ a rotating stage with 4,000 pulses per degree IR, then $\Delta\theta_r \approx 2.5\text{E}(-4)$. Hence, we obtain $\Delta n_1 \approx 3E(-6)$. Roughly speaking, the 7-digit resolution means $\Delta n_1 = 1\text{E}(-6)$. Thus, the resolution of our method is a little less than 7-digit.

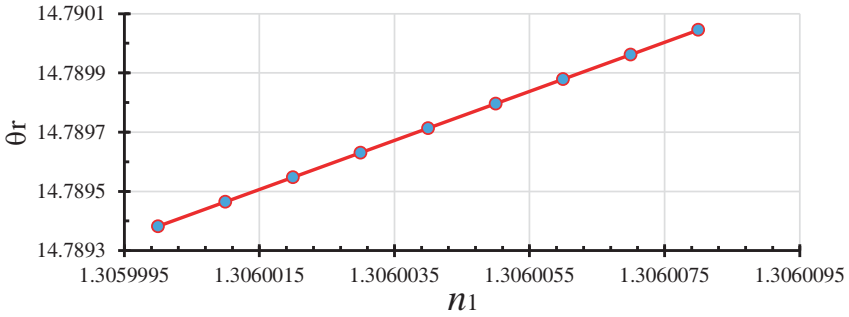

Figure 4. Graph version of Table 2. Note the linear relation and the proportional constant $\Delta\theta_r/\Delta n_1 \simeq 82.9$. Distances between the neighboring scale dots on the axes are: abscissa $4\text{E}(-7)$; and ordinate $1\text{E}(-4)$.

(**EM2**) **Method using Fig. 4**. This is a simple estimation. The distance between neighboring two small dots on the abscissa is $4\text{E}(-7) = 0.0000004$. On the other hand, an example of a seven-digit liquid index usually takes the form like $n_1 = 1.234567$. In these situations, we can say that: provided that the conjecture works, we can use Fig. 4 to find n_1 through θ_r, and the resolution might be no less than 7-digit. We think that an artificial intelligence should be introduced in determination of the index.

4. NUMERICAL EXAMPLES AND DISCUSSION (II): WITH ARTIFICIAL NOISE

So far we did not care much about noise because inclusion of the noise issues would make our problem complicated. The noise, however, is inevitable in experimental works, and we would like to try our elementary Nanotech equipment to reduce the noise. If it works, we will try to improve the equipment. To know the noise effect and to understand the influence of noise, we first prepare a set of data by adding an artificial noise to the solution by the YM. That is, we make a new set of data by adding noises to the original data shown in, for example, Fig. 3(a) or 3(b). As an artificial noise, we employ an additive white Gaussian noise with zero average. We assume three levels of noise classified by their magnitudes: [s] small, SD = min/5; [m] middle, SD = min; and [b] big, SD = 2 × min. Here, min = $\min(\rho_0^{\text{TM}})$ stands for the minimum TM_0 reflection efficiency at $\theta = \theta_r$. To simulate the data obtained through a noisy experiment, we use the superposition of original data by the YM and one of the three levels of noise. We use [s], [m], or [b] in nominating a noise level. To know the influence of noise, we show three pictures in Fig. 5 showing the distortions of the YM result by the superposition of noises [s], [m], and [b].

In the presence of noise, we should consider how to choose the area from which we sample the RC data. Although the points in the close vicinity of θ_r must be important, the efficiency values at these points might have been altered by the noise. Therefore, we employ three kinds of filters (boxes) shown in Fig. 6. This figure displays the same phenomenon as the one in Fig. 3(b). The only difference is the ranges of the coordinates: specifically speaking, the ordinate is from $1.7\text{E}(-6)$ to $3.7\text{E}(-6)$ in Fig. 3(b), while it is from (about) -0 to $2\text{E}(-4)$ in this figure (Fig. 6). The three types of filters are shown as

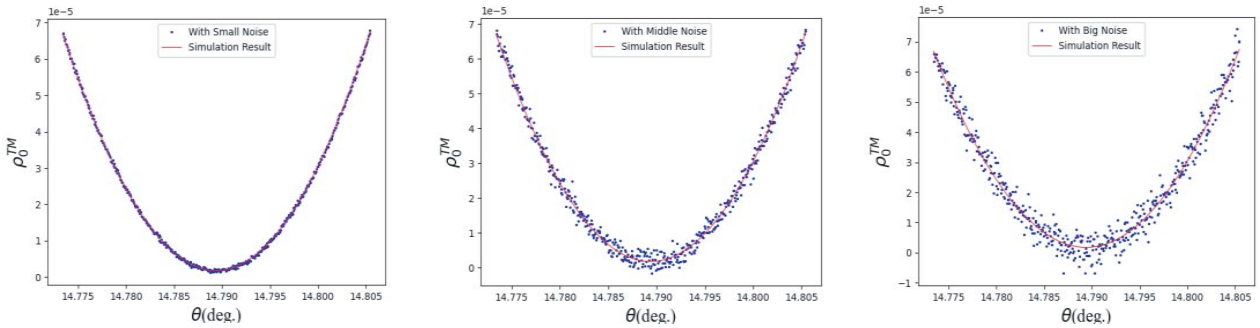

Figure 5. Examples of distortion caused by noises: (a) (left, [s]), (b) (center, [m]), and (c) (right, [b]). The simulation result (red curve) is from a grating mounted similarly as one in Fig. 3.

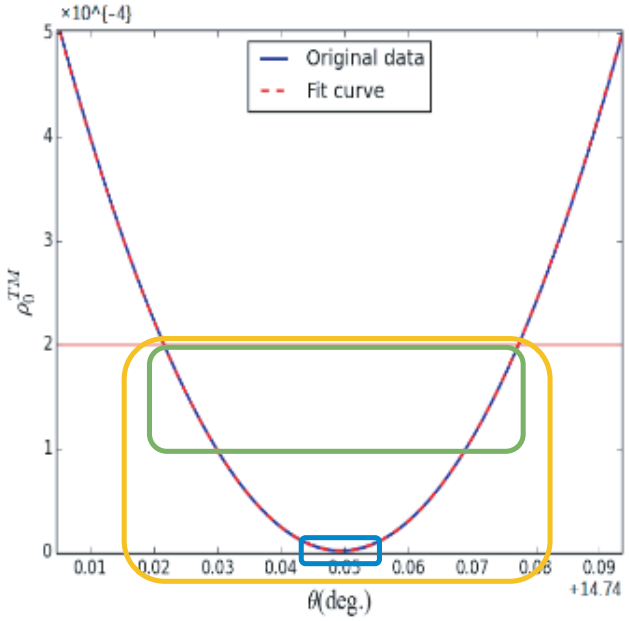

Figure 6. Two RC's and three kinds of filters (boxes). $n_1 = 1.306000$, $\phi = 29.73°$, and $\theta_r = 14.789382°$. The curves [an original data (blue) and a quadratic approximation (red)] show almost the same overlapping as we saw in Fig. 3(b); although the ordinate range is extended.

rectangular boxes with rounded vertexes. Each box is colored by blue, green, or yellow, and the common function of the filters is to choose a necessary number of sampling points from the RC inside the box.*

Let us see the concrete definitions of the filters and the number of sampling points. In our discussions concerning the filters, we call them by their colors like in the following definitions.

- **blue box**: This box focuses on the RC near θ_r, and the definition of the set of sampling-point candidates is given by $\{\theta : |\rho_0^{\mathrm{TM}}(\theta)| \leq 2 \times \min\}$, where min is the minimum TM_0 efficiency.

- **green box**: The definition of this box values the symmetry of the RC near θ_r and hopes to escape from the possible rewriting by noises. Hence, we should neglect the small efficiency part of the RC, and we have chosen the efficiency range $[1.0, 2.0] \times \mathrm{E}(-4)$ after some trial. Note that the data passing through this box include almost nothing from the close vicinity of θ_r.

- **yellow box**: The idea of this box is a union of blue and green: the acceptable range of efficiency

* Please understand that this is no more than a trial. We use the raw data from the filters in data processing to find the shape of RC. We are planning to introduce a window function. Also, we are trying to find filters with good performance.

can be from a tiny negative number [roughly $-1E(-7)$] to $2E(-4)$.

In trial computations we used the data from several hundred sampling points. The points were located on the piece(s) of the RC in one of the boxes. In the following examples, we will find that the green and yellow boxes work well in general, but the blue box is difficult except for the noise [s].

We show in Fig. 7 some results of simulation to compare the performance of the three filters (boxes). The number of sampling points is 600 independent of the box color or the noise level. Probably, we

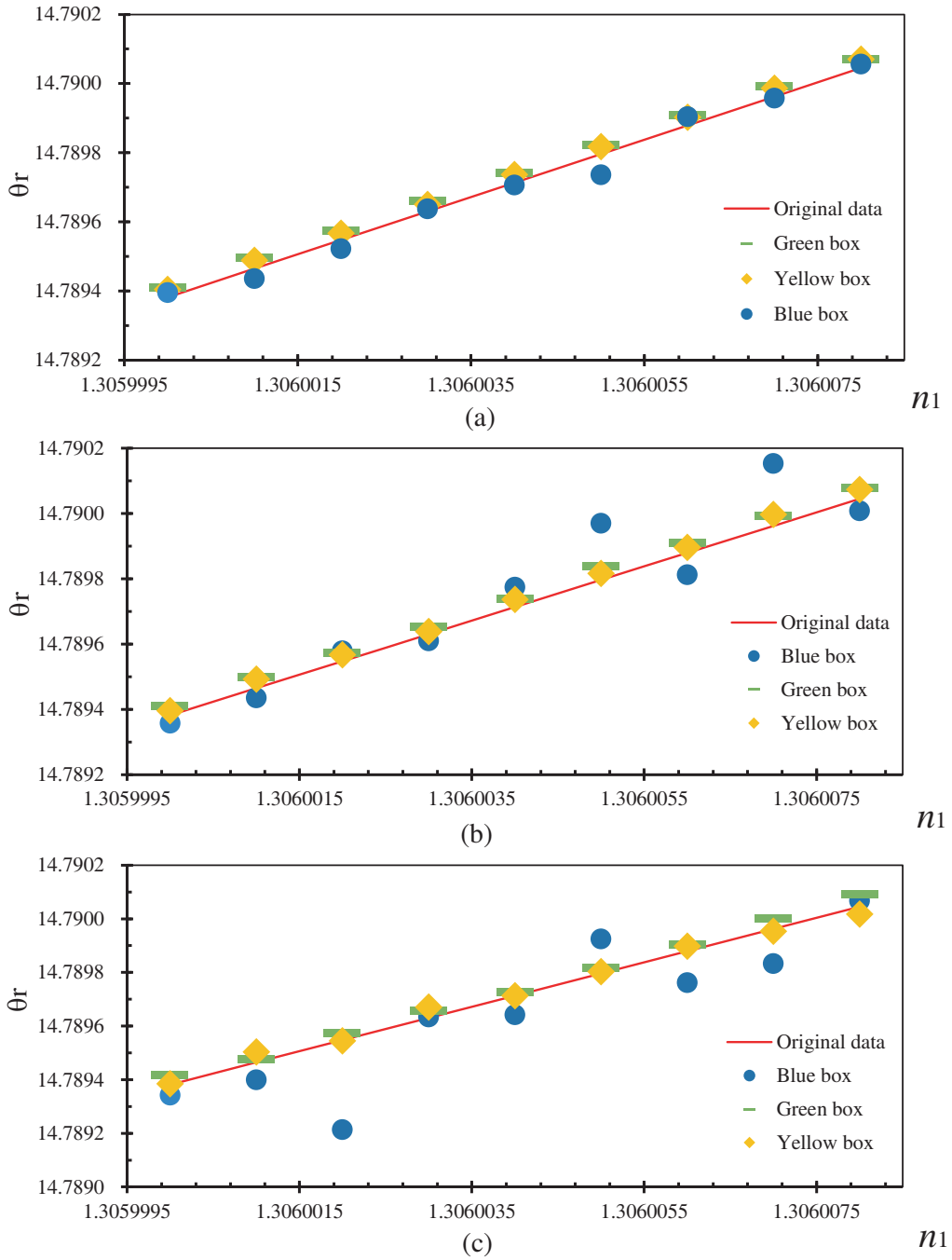

Figure 7. Illustrations of one-to-one correspondence between θ_r and n_1 in the presence of noise. Parameters are the same as those in Fig. 4: $n_{1,rough} = 1.306$, $\phi = 29.73°$. The noise classes are as follows. (a) := [s], (b) := [m], and (c) := [b].

can decrease the number of points. The three illustrations correspond to the three levels of noise: Figs. 7(a), 7(b), and 7(c) display the result of [s], [m], and [b], respectively. First, we observe 7(a), which summarizes the results obtained in the presence of noise [s]. The red straight line is the original data, and the colored points are obtained by our data processing system, which is composed of filter boxes and curve fitting procedure (CFP). This means that the information passed through the filter is the input to the CFP and that the CFP reconstructs an approximation of the RC using the least-squares method (LSM).[♯] Note that the input of the CFP is a part of the RC data and that the reconstructed RC is an analytic curve. In the [s] case, all the boxes work well except for small fluctuation in the blue result and for the tiny upward shifts of the green and yellow marks.[††]

In Figs. 7(b) and 7(c), we find that the green and yellow boxes work well in the environments with [m] or [b] noise. Checking the details, however, we find the green is better than the yellow in the tiny fluctuation. The blue box suffers by comparison with green or yellow as we predicted. As for the possible resolution of our method, we can anticipate that the longest possible significant figures will be seven, but the seventh digit may have a small uncertainty factor depending on the situation.[#]

5. CONCLUSION

As we mentioned in Section 1, we have been working in the development of a grating-coupled plasmon index sensor and have got a few research findings on the sensor structure and directions for using it. This article explained the present situation together with the knowledge. Also, this article examined the achievable resolution of the sensor a few times. In Subsection 3.3, we tried two times and got inconsistent results: (**EM1**) used the proportional relation $\Delta n_1 = \Delta\theta_r/82.9$ and concluded that our result was a little below the target (7-digit); on the other hand, (**EM2**) examined the enlarged figure and recognized that our method could determine no less than 7-digit. We are discussing to introduce the AI technology for this issue.

We have been preparing this report of our research work, which is focused mainly on the theoretical part of the sensor development. If we call our past study *the first step*, then we move into *the second step* after submission of this manuscript according to our schedule. The second step will continue a few years where we hope to deal mainly with the practical issues. At the same time, we have to consider the problem above. Hence, the probable subjects of our second step will be as follows:

1. Another article: We are writing another article on a selectable range of the min, the TM_0 reflection efficiency at $\theta = \theta_r$. This allows to employ a bigger value, e.g., $1E(-3)(= 0.1\%)$ or further as the minimum efficiency. This makes experiment and data processing easier than before.

2. A carry over problem: We continue to consider how to maintain the stability of the sensor.

3. Investigation and examination of the variety of components for verification by experiment: Specifically, the components include: grating profile and material, light source, artificial noise, geometry of the noise filter, refractive index standard, etc.

4. Improvement of environment for precision measurement: This will be a tough work, and we need joint research for this subject.

APPENDIX A. A METHOD TO GET THE RECOMMENDED AZIMUTH ANGLE

To get recommendable or proper azimuth angles, we should make a systematic survey of the $n_{1,rough}$- and ϕ-dependence of the resonance absorption strength. As widely known, strong absorption spends a greater part of incident power to excite the plasmon surface wave and to generate TE modes for the boundary conditions. Consequently, the return-signal (the reflection efficiency) is usually small, and sometimes, photo-detectors fail to catch the signal. Hence, our target is to find the return-signal with proper strength for data processing.

[♯] Although we usually look for parabola (quadratic) approximations, inclusion of higher-order terms in the approximation may be useful to deal with small asymmetry of the RC. This will be one of our future subjects.

[††] We know the root cause of this problem, and we can make compensation if we have sufficient data for comparison.

[#] Assuming a tiny error of θ_r in Fig. 7, we predicted the error in n_1. Using this result, we can conclude that an acceptable error of θ_r is $5E(-5)$ to endorse the 7-digit resolution.

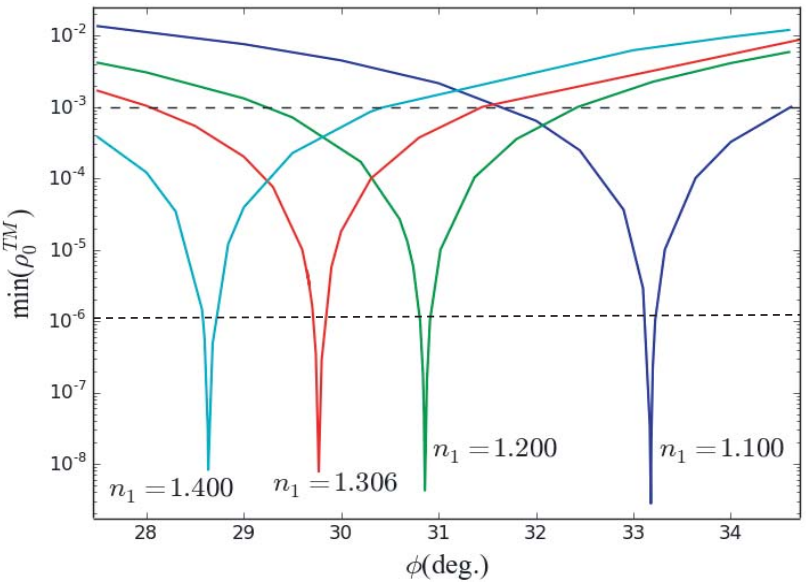

Figure A1. The minimum efficiency $\rho_0^{\mathrm{TM}}(\theta_r)$ as a function of ϕ. There are four curves corresponds to four values of n_1. Note that the n_1 values should have additional three zeros: $1.306 \rightarrow 1.306000$.

Figure A1 shows the strength of the minimum return-signal as a function of the azimuth angle ϕ (abscissa) and refractive index n_1 (parameter). When we use this figure, we first draw a horizontal line like two broken lines that we see at 1E(−3) and 1E(−6). Finding the intersection points with the n_1 curve, we get the candidates. We add some comments:

1. Usually, the first-time try is not enough, and we should repeat the same procedure (with narrower n_1 ranges) a few times.

2. There are two ϕ's (ϕ_1 and ϕ_2) for a given value of efficiency. Therefore, we should examine which combination ($n_{1,rough}$, ϕ) ($\phi = \phi_1$, ϕ_2) works better.

3. When Fig. A1 is not clear to read in detail, we use a similar figure whose ordinate shows the reciprocal of the minimum efficiency $1/\rho_0^{\mathrm{TM}}(\theta_r)$. This modified version is easier to read sometimes.

4. Although we define $n_{1,rough} = 1.235$, we use $n_1 = 1.234567$ in YM numerical computations. Usually, the results using 1.235000 and the one using 1.234567 are not so different. Hence, this rule is for uniformity.

REFERENCES

1. Raeter, H., "Surface plasmon and roughness," V. M. Argranovich and D. L. Mills (eds.), *Surface Polaritons*, Chapter 9, 331–403, North-Holland, New York, Amsterdam, 1982.
2. Nevière, M., "The homogeneous problem," R. Petit (ed.), *Electromagnetic Theory of Gratings*, Chapter 5, 123–157, Springer-Verlag, Berlin, Heidelberg, New York, 1980.
3. Okuno, Y., T. Suyama, R. Hu, S. He, and T. Matsuda, "Excitation of surface plasmons on a metal grating and its application to an index sensor," *IEICE Trans. Electron.*, Vol. 90, No. 7, 1507–1514, 2007.
4. Luo, Z., T. Suyama, X. Xu, and Y. Okuno, "A grating-based plasmon biosensor with high resolution," *Progress In Electromagnetics Research*, Vol. 118, 527–539, 2011.
5. Matsuda, T., D. Zhou, and Y. Okuno, "Numerical analysis of plasmon resonance absorption in bisinusoidal metal gratings," *J. Opt. Soc. Amer. A*, Vol. 19, 695–701, 2002.
6. Wood, R. W., "On a remarkable case of uneven distribution of light in a diffraction grating spectrum" *Lond. Edinb. Dublin Philos. Mag. J. Sci.*, Vol. 4, 396–402, 1902, doi: 10.1080/14786440209462857.

7. Rayleigh, L., "On the dynamical theory of gratings" *Proc. R. Soc. Lond. A.*, Vol. 79, 399–416, 1907, doi: 10.1098/rspa.1907.0051.
8. Fano, U., "The theory of anomalous diffraction gratings and of quasi-stationary waves on metallic surfaces (Sommerfeld's Waves)," *J. Opt. Soc. Am.*, Vol. 31, 213–222, 1941, https://www.osapublishing.org/josa/abstract.cfm?.
9. Maystre, D., "Theory of Wood's anomalies" Enoch S. and Bonod N. (eds), *Plasmonics: From Basics to Advanced Topics.*, 1st Edition, 39–83, Springer, Berlin/Heidelberg, Germany, 2012.
10. Taniguchi, N., "On the basic concept of 'Nano-Technology'," *Proc. Intl. Conf. Prod. London, Part II British Society of Precision Engineering*, 1974.
11. Homola, J., S. Yee, and G. Gauglitz, "Surface plasmon resonance sensors: review," *Sensors Actuators B*, Vol. 54, 3–15, 1999.
12. Homola, J., I. Koudela, and S. Yee, "Surface plasmon resonance sensors based on diffraction gratings and prism couplers: sensitivity comparison," *Sensors Actuators B*, Vol. 54, 16–24, 1999.
13. Matsushima, A., T. Matsuda, and Y. Okuno, "Introduction to Yasuura's method of modal expansion with application to grating problems," *The Generalized Multipole Technique for Light Scattering*, T. Wriedt and Y. Eremin (eds.), Chapter 8, 51 pages, Springer, 2018.
14. Suyama, T., Z. Qian, F. Shi, H. Enomoto, and A. Matsushima, "Improvement of resolution of liquid refractive index measurement using metallic grating," *Progress In Electromagnetics Research M*, Vol. 85, 29–38, 2019.
15. Xu, X., Y. Okuno, and T. Suyama, "Analysis of plasmon resonance in a multilayer-coated bigrating," *PIERS Proceedings*, 1318–1322, Guangzhou, China, Aug. 25–28, 2014.
16. Gong, R., B. W. Chen, X. Xu, and Y. Okuno, "Resolution of a grating-based plasmon index sensor with efficiency-alone interrogation," *2016 Progress In Electromagnetic Research Symposium (PIERS)*, 4062–4066, Shanghai, China, Aug. 8–11, 2016.
17. Zheng, M., X. Xu, R. Gong, and Y. Okuno, "A grating-based plasmon index sensor: performance simulation in the presence of noise," *2017 Progress In Electromagnetics Research Symposium — Fall (PIERS — FALL)*, 2193–2198, Singapore, Nov. 19–22, 2017.
18. Matsuda, T., X. Xu, and Y. Okuno, "A couple of topics in numerical analysis of diffraction by a metal grating using Yasuura's method of modal expansion," *PIERS Proceedings*, 1930–1934, Prague, Chez Republic, 2015.
19. Hass, G. and L. Hardy, "Optical properties of metals," D. G. Gray (ed.), *American Inst. Phys. Handbook*, 2nd Edition, 6–107, McGraw-Hill, NY, 1963.
20. Palik, E. D., *Handbook of Optical Constants of Solids*, Academic Press, Boston, 1998.
21. Johnson, P. B. and R. W. Christy, "Optical constants of the noble metals," *Phys. Rev. B*, Vol. 6, 4370, Published Dec. 15, 1972.
22. Rakik, A. D., A. B. Djurisic, J. M. Elazar, and M. L. Majewski, "Optical properties of metallic films for vertical-cavity optoelectronic devices," *App. Opt.*, Vol. 37, 5271–5283, 1998.
23. Bryan-Brown, G. P., J. R. Sambles, and M. C. Hutley, "Polarization conversion through the excitation of surface plasmons on a metallic grating," *J. Modern Opt.*, Vol. 37, 1227–1232, 1990.
24. Matsuda, T., D. Zhou, and Y. Okuno, "Numerical analysis of TE-TM mode conversion in a metal grating placed in conical mounting," *IEICE Trans. Electron.*, Vol. J82-C-I, 42–49, 1999 (in Japanese).